Available online at www.sciencedirect.com
SCIENCE DIRECT
Journal of Catalysis 237 (2006) 303–313
JOURNAL OF CATALYSIS
www.elsevier.com/locate/jcat

Effects of the structure of ceria on the activity of gold/ceria catalysts for the oxidation of carbon monoxide and benzene

Suk-Yin Lai [a,*], Yongfu Qiu [a], Shuiju Wang [b]

[a] *Department of Chemistry and Centre for Surface Analysis and Research, Hong Kong Baptist University, Kowloon Tong, Hong Kong, China*
[b] *State Key Laboratory for Physical Chemistry of Solid Surface, Xiamen University, Xiamen, 361005, China*

Received 12 September 2005; revised 17 November 2005; accepted 18 November 2005

Available online 13 December 2005

Abstract

Using precipitated cerium hydroxide dried at 100 °C as the support, highly dispersed ceria-supported gold catalyst was prepared. Compared with similarly prepared catalysts supported on low-surface area ceria, gold on the high-surface area support showed more resistance to sintering and was more active toward the oxidation of CO and benzene. The oxidation of benzene was very dependent on the structure of ceria. Temperature-programmed reduction showed that the reducibility of surface oxygen was higher for high-surface area ceria. It is proposed that the creation of surface oxygen vacancies by ceria surface reduction promoted oxygen adsorption. Active oxygen formed by dissociation of the adsorbed oxygen is the active species for benzene oxidation, and the dissociation is promoted by gold nanoparticles. When present together in the reactant mixture, benzene inhibited the oxidation of CO, but CO enhanced the oxidation of benzene. Moisture had a promoting effect on both CO and benzene oxidation.

Keywords: Gold; Ceria; CO oxidation; Benzene oxidation

1. Introduction

Gold has long been accepted as a chemically inert metal of little significance in catalysis. However, since the discovery of the excellent activity of highly dispersed gold for CO oxidation by Haruta et al. [1], studies on the catalytic properties of nanogold materials have proliferated. Gold shows other interesting catalytic properties besides CO oxidation [2–4]. Properly prepared gold catalysts on suitable support exhibit unique properties for hydrogenation reactions [5,6], selective oxidation of CO in hydrogen [7,8], formation of hydrogen peroxide from oxygen and hydrogen [9], epoxidation of olefins with hydrogen and oxygen [10,11], the water–gas shift reaction [12,13] and reactions for the abatement of automobile pollution [14,15].

In addition to carbon monoxide, volatile organic compounds (VOCs), of which benzene is one, constitute an important source of urban air pollution. Catalytic oxidation is one method used to remove VOCs. Because of its favorable redox properties, ceria has been used as an oxidation catalyst [16–18]. It is also an important component of three-way catalysts for automobiles. The ability of CeO_2 to catalyze oxidation reactions has prompted studies on its use in gold-based catalysts. Au/CeO_2 was found to have high activity and stability for selective CO oxidation in hydrogen [8]. Adding ceria was found to promote oxidation reactions on gold supported on alumina [15,19]. Gold supported on ceria was found to be quite active for the oxidation of VOCs [20]. $Gold/CeO_2$ prepared by deposition–precipitation was slightly more active than $gold/Fe_2O_3$ prepared by coprecipitation for toluene oxidation [21]. Likewise, gold–ceria catalysts promoted by vanadia was more active than gold–titania or gold–zirconia promoted by vanadia [22,23]. These results demonstrate that ceria-supported gold can be a useful catalyst for the oxidation of volatile organic compounds.

The activity of ceria-based catalyst is known to depend greatly on its structure. Nanosized ceria shows higher activity than bulk-phase ceria, because of the easier reduction of the surface oxygen species on ceria nanoparticles [18,24]. Gold supported on nanocrystalline ceria was recently found to exhibit

* Corresponding author. Fax: +852 34117348.
E-mail address: laisy@hkbu.edu.hk (S.-Y. Lai).

0021-9517/$ – see front matter
doi:10.1016/j.jcat.2005.11.020

excellent activity for CO oxidation [25]. In this paper we report the result of our investigation into the activity of gold supported on two ceria samples with very different specific surface areas for CO and benzene oxidation with the objective of determining the influence of the structure of ceria on the structure of the supported gold particles and the catalytic activity for both reactions and on their susceptibility to deactivation by sintering. To evaluate the potential application of the catalyst in ambient air, the catalytic activity when both CO and benzene were present together, with or without moisture, was also examined.

2. Experimental

2.1. Catalyst preparation

The low-surface area ceria (denoted as CeO_2-LS) was obtained from Shanghai Chemical Corporation. To produce high-surface area ceria-supported catalysts, cerium hydroxide was precipitated from a solution of 0.22 M cerium (III) nitrate hexahydrate solution by adding 28% aqueous ammonia. The precipitate was washed three times with deionized water and then dried at 100 °C for 20 h. Portions of the dried precursor and the commercial ceria were calcined to 300, 500, or 700 °C for 6 h. These were denoted as CeO_2-HS-T and CeO_2-LS-T, where T is the temperature of calcination (°C). Gold was loaded onto the as-received commercial ceria and the dried precipitated ceria precursor by deposition–precipitation. The pH of a suspension of the support and the pH of a solution of chloroauric acid in deionized water were separately adjusted to 10 with sodium hydroxide. The two were then combined and stirred for 5 h at room temperature. (Using ammonia for pH adjustment should be avoided, due to the hazard of the formation of explosive fulminating gold [26].) The suspensions were then filtered and dried at 100 °C for 12 h. Separate portions were then calcined at 300, 500, or 700 °C for 6 h. The catalysts were denoted as Au/CeO_2-HS-T or Au/CeO_2-LS-T.

2.2. Catalyst characterization

The specific surface area of the catalysts was determined by nitrogen adsorption at 77 K with a NOVA 1200 automatic adsorption apparatus. The gold content in the catalysts were determined by dissolving the gold from the catalysts with aqua regia and then analyzing the catalysts by ICP-AES using a Perkin-Elmer Optima 3000 spectrometer. The crystal phases present in the catalysts were determined by powder X-ray diffraction (XRD) using a Rigaku D-max X-ray diffractometer with Ni-filtered Cu-K_α radiation. The catalyst surface compositions were determined by X-ray photoelectron spectroscopy using a Leybold Heraeus-Shengyang SKL-12 electron spectrometer equipped with a VG CLAM 4 MCD electron energy analyzer, with Al-K_α as the excitation source. The morphology of the catalysts was studied by transmission electron microscopy with a FEI TECNAI field emission high-resolution electron microscope at an electron beam energy of 300 kV.

2.3. Temperature-programmed reduction

Temperature-programmed reduction (TPR) was performed in a flow reaction system. For each run, 0.3 g of catalyst was first oxidized in a flow of synthetic air for 30 min at 300 °C for the gold-containing samples and at 500 °C for the oxide supports. The sample was then cooled to 100 °C, flushed with nitrogen at 100 °C for 30 min, and cooled to room temperature in nitrogen. The flow was then switched to a 10% H_2 in N_2 mixture. A gas flow rate of 50 mL min^{-1} was established, and the temperature of the catalyst bed was raised to 900 °C at a rate of 10 °C min^{-1}. The effluent gas was first passed through a liquid nitrogen cold trap to remove water vapor and then analyzed with a Gow-Mac thermal conductivity detector.

2.4. Fourier transform infrared spectroscopy

The Fourier transform infrared (FTIR) spectra of adsorbed CO on the catalysts were studied using a flow-through infrared cell with a CaF_2 window. The catalysts were pressed into self-supporting wafers, pretreated in flowing synthetic air at 300 °C for 2 h, then cooled to −140 °C in nitrogen. For CO adsorption, the wafers were allowed to contact a flowing stream of 5% CO in nitrogen for 10 min. The cell was then flushed with flowing nitrogen for 10 min to remove gaseous CO. The spectra were measured in the transmission mode with a Nicolet Magna-IR 500 spectrometer with a MCT detector at a resolution of 4 cm^{-1} with 128 scans.

2.5. Catalytic activities

The catalytic activities of the catalysts for CO oxidation and benzene oxidation were studied using a laboratory-scale flow reactor system. (Note: Both CO and benzene are highly toxic, and benzene is highly carcinogenic; precautions must be taken while handling them.) In each run, 0.2 g of the catalyst diluted with 0.2 g of silica gel was first activated in synthetic air at 300 °C for 2 h. Then 1% CO in air at a total flow rate of 50 mL min^{-1} or 0.5% benzene in air at a flow rate of 200 mL min^{-1} was passed over the catalyst at different temperatures, and the products were analyzed using two Shimadzu 8A gas chromatographs. One of these devices, equipped with a thermal conductivity detector, a 13X molecular sieve, and a Porapak Q column, was used to determine CO, N_2, O_2, and CO_2. The other, equipped with a flame ionization detector and a Porapak Q column, was used to analyze benzene. In addition to measuring the activity of the catalyst for the individual reactions, one of the most active catalysts was tested for the oxidation of CO and benzene (1% CO, 0.5% benzene, balance synthetic air; total flow, 200 mL min^{-1}) in the presence or absence of 3% water. For comparison, a World Gold Council reference catalyst (type A, Au/TiO_2, 1.5 wt% gold), was also studied under similar conditions.

Table 1
Gold loading and specific surface area of the catalysts

Sample	Gold loading (wt%)	S_{BET} after calcination at different temperature ($m^2\ g^{-1}$)		
		300 °C	500 °C	700 °C
CeO_2-LS	–	6.7	6.7	5.5
Au/CeO_2-LS	0.7	7.0	6.3	6.4
CeO_2-HS	–	65.5	60.7	29.1
Au/CeO_2-HS	1.5	84.6	78.7	43.0

3. Results and discussion

3.1. Catalyst characterization

All of the samples showed the same powder XRD pattern, which matched that of CeO_2 with cubic fluorite structure. The width of the diffraction peaks of the HS series was much broader than that of the LS series, demonstrating that the CeO_2 particles from the precipitated precursors were much smaller than those from the commercial source. Diffraction peaks from gold could hardly be detected because of the low gold loading.

The specific surface areas of the supports, as well as the gold catalysts after calcination at different temperatures and the gold loading as determined from ICP-AES, are given in Table 1. For the LS catalyst series, the specific surface area of CeO_2 was rather low and showed only small changes after calcination even at 700 °C. The addition of gold also had only small effect on the catalyst surface area, indicating that the commercial ceria is already well calcined. The specific surface area of CeO_2-HS calcined to 300 °C was nearly 10 times that of CeO_2-LS. It decreased slightly (by 7%) with increasing calcination temperature from 300 to 500 °C. Raising the calcination temperature to 700 °C led to a much greater decrease in specific surface area. Adding gold to the precipitated ceria before calcination inhibited sintering, causing the gold-loaded catalysts to have a higher specific surface area than the support calcined at the same temperature. This effect is particularly noticeable in the sample calcined at 700 °C. The high-surface area support was able to take up more gold from solution, resulting in higher gold loading in the catalysts.

Representative transmission electron micrographs for the CeO_2-HS-300, Au/CeO_2-HS-300, and Au/CeO_2-LS-300 samples are shown in Fig. 1. The low-resolution electron micrograph shows that the ceria is composed of small (7–14 nm) overlapping particles. Similar ceria particles were also observed with the Au/CeO_2-HS-300 catalyst. Although slightly darker particles of about 4 nm could be discerned, whether they were gold or smaller ceria particles from the contrast only was difficult to determine. A high-resolution study, using the spacing of the lattice fringes for identification, was tried. A 4.5-nm gold particle on the Au/CeO_2-HS-300 is marked in Fig. 1e; however, such particles were difficult to find and likely are not really representative. Most of the gold particles could be much smaller and not detectable. The dimensions of the low-surface area ceria particles are much larger. The polygonal-shaped particles were $\geqslant$23 nm in diameter. Gold particles 5–7 nm in diameter can be readily distinguished from the support. The high-resolution electron micrograph in Fig. 1f shows gold particles topped with the (111) lattice plane attached to the (111) face of a large ceria particle. The identification of the marked particle in Fig. 1d and e as CeO_2 and metallic gold, respectively, was supported by measurement of the lattice spacing and by the digital electron diffraction pattern shown in the insets.

XPS revealed the presence of oxygen, cerium, and gold on all of the catalysts. Sodium was not detected on any of the samples, and a small amount of chlorine was found only on the Au/CeO_2-HS-300 catalyst. With this catalyst, the chlorine peak disappeared after the catalyst was used for the CO oxidation reaction. The surface concentrations of gold, cerium, and oxygen measured from the area of the Au 4f, Ce 3d, and O 1s peaks are given in Table 2. Because the concentration of adventitious carbon was rather variable, it was excluded from the calculation of composition. For both catalyst series, the ratio of surface concentration of gold to cerium decreased on increasing calcination temperature, showing a decrease of gold dispersion with calcination temperature. This gold sintering effect was more severe for the LS series.

The cerium 3d peak showed the typical multiplet structure found for cerium dioxide [27]. To correct for charging effect, the binding energies of the XPS peaks were calculated with the Ce u‴ peak set at 917.0 eV, as described previously [28]; the results are given in Table 3. The main O 1s peak at 529.3–529.4 eV (O_L) was assigned to lattice oxygen of CeO_2. A higher binding energy shoulder was found for all samples at about 532 eV; this was assigned to a mixture of surface hydroxyl and carbonate groups. Whereas the binding energies for Ce 3d and O 1s peaks were nearly identical, the peaks were broader for the HS series samples than for the LS series samples. This again reflects the smaller CeO_2 particle size of the HS samples. The surfaces of small particles were more heterogeneous, with more surface atoms at corner and edge sites that are in slightly different chemical environments than those on the well-developed crystal surfaces that dominate for the large CeO_2 crystals.

A larger variation of the Au 4f spectra with the nature of the support and the temperature of calcination was observed. Apart from a main Au 4f doublet, a higher binding energy peak or shoulder could be found for the HS series catalyst but not for the LS series. The binding energy of the main Au 4f doublet shifted to lower values with increasing calcination temperature, gradually separating itself from the higher-binding energy component. In resolving the gold peaks by curve fitting, it was assumed that the higher-binding energy species was a cationic species with a fixed binding energy of 86.0 eV, a value close to that reported for Au_2O_3 [29]. The results are shown in Fig. 2. Note that the binding energy for Au 4f obtained for the main peak was lower than the value of 84 eV for bulk metal. The lowest binding energy was found with Au/CeO_2-LS-700, the sample that should have the largest gold particle size. The low gold binding energy found should be attributed to a charge transfer from support to gold, similar to the case of Au/TiO_2 discussed by Arrii et al. [30]. The shift toward higher binding energy with decreasing particle size, especially for the HS series, possibly

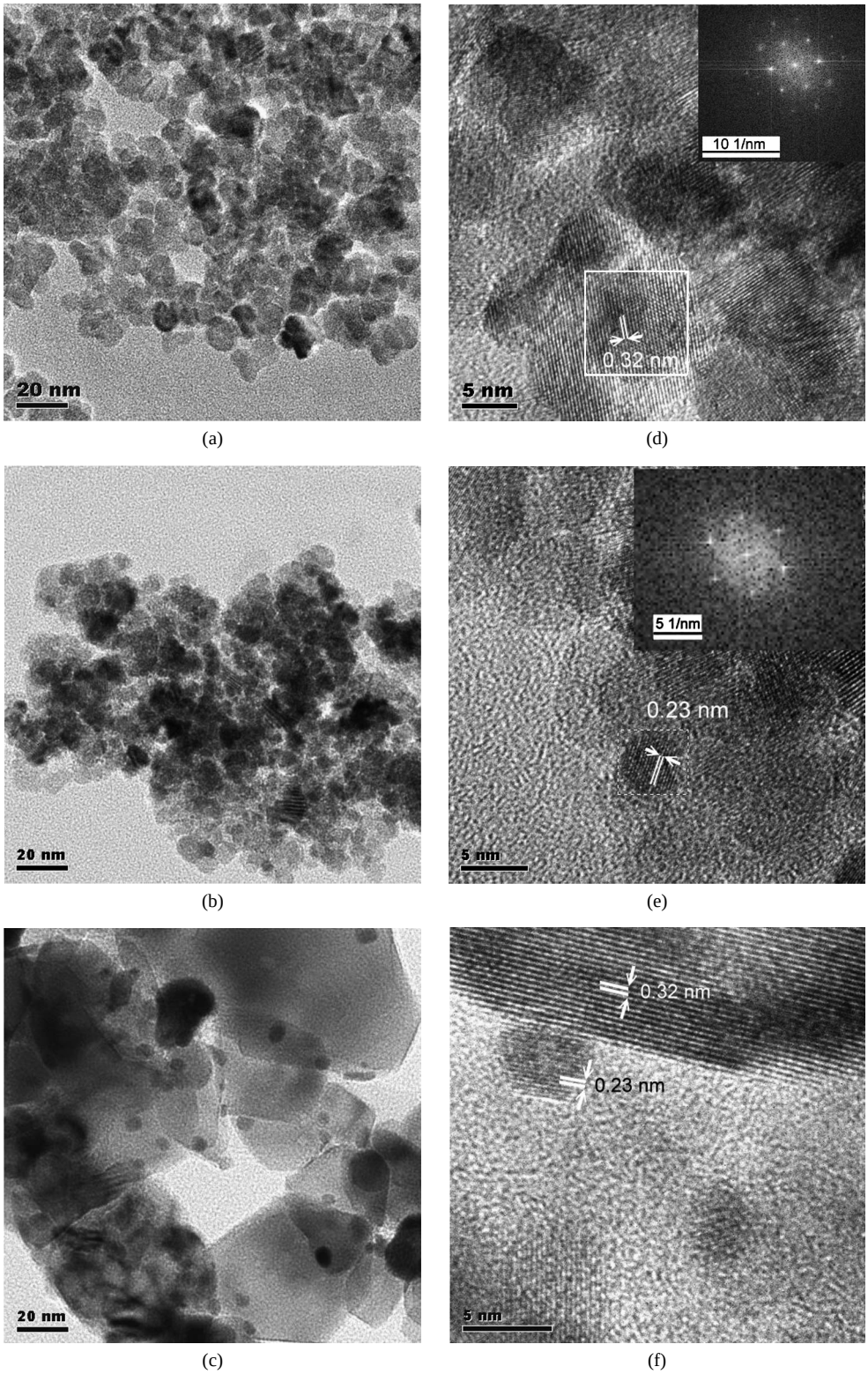

Fig. 1. Transmission electron micrographs of the 300 °C calcined catalysts. (a)–(c), low resolution micrographs; (d)–(f), high resolution micrographs. (a), (d), CeO_2-HS-300; (b), (e), Au/CeO_2-HS-300; (c), (f), Au/CeO_2-LS-300. Insets: digital electron diffraction patterns of the marked particles.

resulted from a final state effect of reduced screening of the core hole for small metal particles. The higher Au 4f binding energy for the fresh Au/CeO_2-HS-300 sample compared with the sample after reaction may be caused by an electron-withdrawing effect of residual Cl.

3.2. TPR

The TPR profiles of the samples CeO_2-LS-300, CeO_2-HS-300, Au/CeO_2-LS-300, and Au/CeO_2-HS-300 are shown in Fig. 3. The TPR profile of CeO_2-LS-300 is similar to those

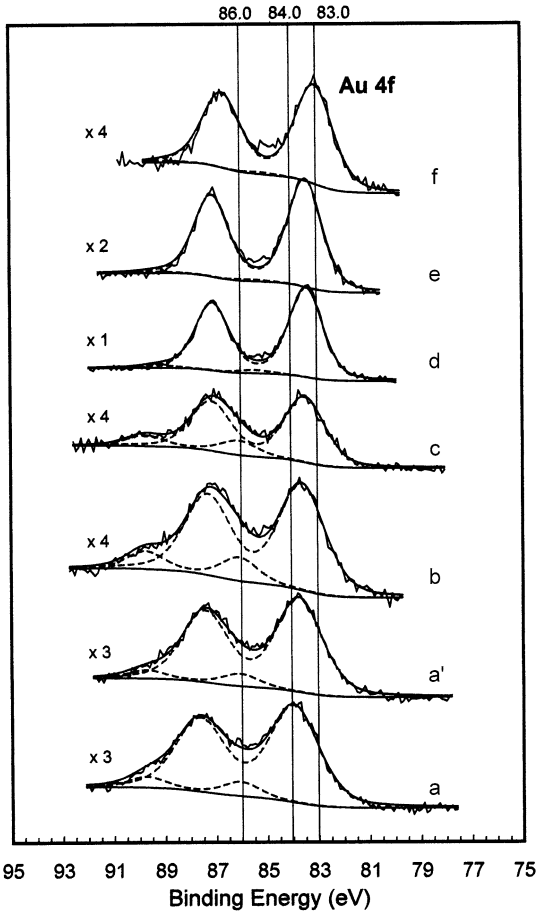

Fig. 2. Au 4f XPS spectra of the catalysts. (a) Au/CeO_2-HS-300, (b) Au/CeO_2-HS-500, (c) Au/CeO_2-HS-700, (d) Au/CeO_2-LS-300, (e) Au/CeO_2-LS-500, (f) Au/CeO_2-LS-700, (a′) Au/CeO_2-HS-300 after CO oxidation reaction.

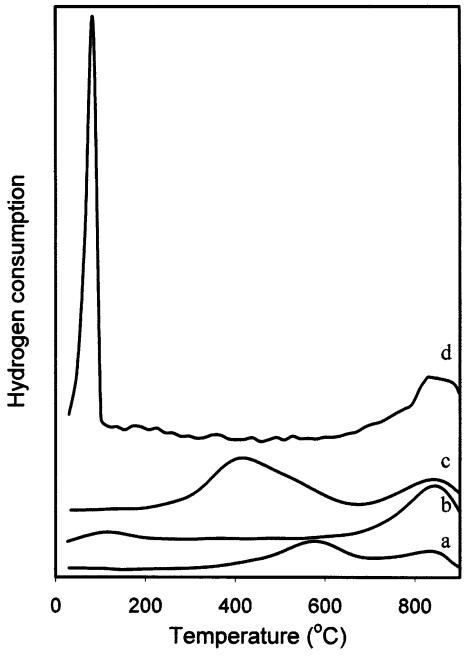

Fig. 3. TPR profiles of the catalysts. (a) CeO_2-LS-300, (b) Au/CeO_2-LS-300, (c) CeO_2-HS-300, (d) Au/CeO_2-HS-300.

Table 2
Surface composition of the catalysts

Catalyst	Ce (mol%)	O (mol%)	Au[a] (mol%)	Cl (mol%)	Au/Ce (mole ratio)
Au/CeO_2-LS-300	25.7	73.0	1.3 (0.04)	0	0.051
Au/CeO_2-LS-500	25.8	73.4	0.8 (0.01)	0	0.031
Au/CeO_2-LS-700	29.5	70.2	0.3 (0)	0	0.010
Au/CeO_2-HS-300	32.3	65.3	0.7 (0.08)	1.6	0.021
Au/CeO_2-HS-500	28.6	70.9	0.5 (0.08)	0	0.017
Au/CeO_2-HS-700	28.9	70.8	0.3 (0.05)	0	0.010
Au/CeO_2-HS-300-AR	28.8	70.5	0.6 (0.07)	0	0.023

[a] Total surface concentration, the concentration of the higher binding energy component is given in the parenthesis.

Table 3
Binding energy of different elements on the catalyst surface

Catalyst	Ce u‴		O 1s (O_L)		Au $4f_{7/2}$	
	BE (eV)	FWHM (eV)	BE (eV)	FWHM (eV)	BE (eV)	FWHM (eV)
Au/CeO_2-LS-300	916.7	2.2	529.3	1.7	83.1	1.5
Au/CeO_2-LS-500	916.7	2.2	529.4	1.7	83.2	1.6
Au/CeO_2-LS-700	916.7	2.3	529.4	1.8	83.0	1.7
Au/CeO_2-HS-300	916.7	2.7	529.3	2.0	83.6	2.2
Au/CeO_2-HS-500	916.7	2.6	529.3	2.0	83.3	2.1
Au/CeO_2-HS-700	916.7	2.3	529.3	2.0	83.2	1.9
Au/CeO_2-HS-300-AR	916.7	2.6	529.4	2.0	83.4	2.0

reported in the literature. The low-temperature reduction peak at 570 °C and the high temperature peak at 830 °C were typically interpreted as the reduction of surface-capping oxygen and bulk-phase lattice oxygen, respectively [31]. With CeO_2-HS, the position of the bulk lattice oxygen reduction peak remained the same, but the surface reduction showed a downward shift of 165 to 405 °C, similar to that reported by Venezia et al. for ceria of similar surface area [32] and in agreement with the prediction of the enhancement in reducibility for nanosized ceria obtained by theoretical computation methods [33,34]. When gold was added, the lower temperature reduction peak shifted further to the low value of 130 °C for Au/CeO_2-LS-300 and 83 °C for Au/CeO_2-HS-300. Scirè et al. suggested that gold weakens the adjacent surface Ce–O bond [20]. On the other hand, Gluhoi et al. reported that nanogold supported on alumina facilitates the H_2/D_2 exchange reaction even at room temperature [35]. We believe that the effect of gold observed here should be due to hydrogen activation on gold and subsequent spillover of the reactive atomic hydrogen onto the ceria surface at low temperature. Because most of the gold was in the metallic state and the surface coverage of gold was very low (only 1.3% for Au/CeO_2-LS and 0.7% for Au/CeO_2-HS), surface oxygen in close proximity to the gold particles should account only for a small fraction of the total, and a reduction peak at the regular reduction temperature for CeO_2 distant from the gold particle should still be found if surface oxygen-bond weakening was the major effect.

3.3. FTIR

We found that the adsorption of CO on the catalysts was very weak; no CO bands were found when adsorption was car-

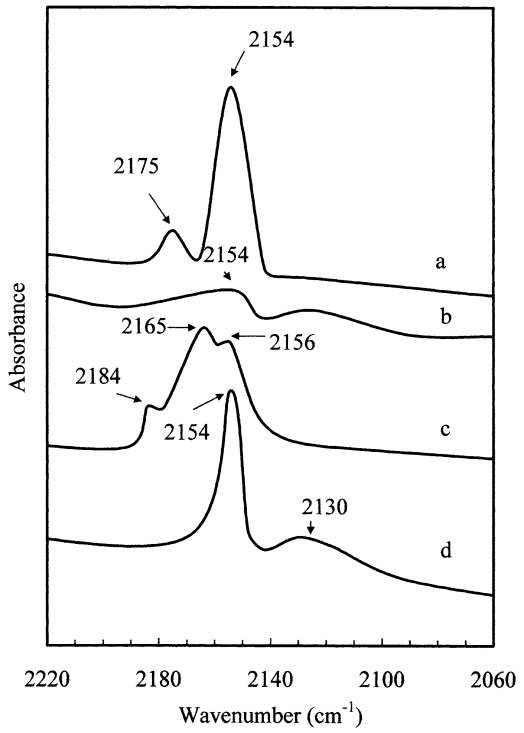

Fig. 4. FTIR spectra of adsorbed CO at −140 °C on the HS series catalysts. (a) CeO_2-HS-500, (b) CeO_2-HS-300, (c) Au/CeO_2-HS-300, (d) Au/CeO_2-HS-500.

ried out at room temperature. The FTIR spectra of adsorbed CO on selected samples of the HS series at −140 °C are shown in Fig. 4. Ceria calcined to 300 °C showed only a very weak CO absorption band at 2154 cm^{-1}, whereas on the sample calcined to 500 °C, the band at 2154 cm^{-1} was much more intense and another band at 2175 cm^{-1} appeared. Bands around 2154 cm^{-1} had been assigned to weakly adsorbed CO, either through van der Waal's force or by hydrogen bonding to surface OH species [36]. The higher-frequency band was assigned to CO bound to Lewis acid sites of coordinatively unsaturated Ce^{4+} [36]. The FTIR spectra of the regions above 3000 cm^{-1} and below 1600 cm^{-1} (not shown here for brevity) indicated that much higher amounts of water and carbonate species were present on the 300 °C calcined sample, blocking the sites for CO adsorption. On Au/CeO_2-HS-300, CO adsorption bands were found at 2156, 2165, and 2184 cm^{-1}. We attributed the 2156 cm^{-1} peak to weakly adsorbing CO similar to the one producing the 2154 cm^{-1} band on CeO_2-500. Because a small amount of chloride was detected on this sample by XPS, the bands at 2165 and 2184 were tentatively assigned to CO adsorbed on ceria sites adjacent to chloride ions [37] rather than to adsorbed CO associated with cationic gold, because XPS revealed cationic gold in similar surface concentration for Au/CeO_2-HS-300 and Au/CeO_2-HS-500 but we did not detect these bands on Au/CeO_2-HS-500. Compared with the pure support calcined at the same temperature, much less adsorbed water and carbonate were detected on the Au/CeO_2-HS-300, showing that gold facilitates their desorption from ceria, allowing absorption of CO.

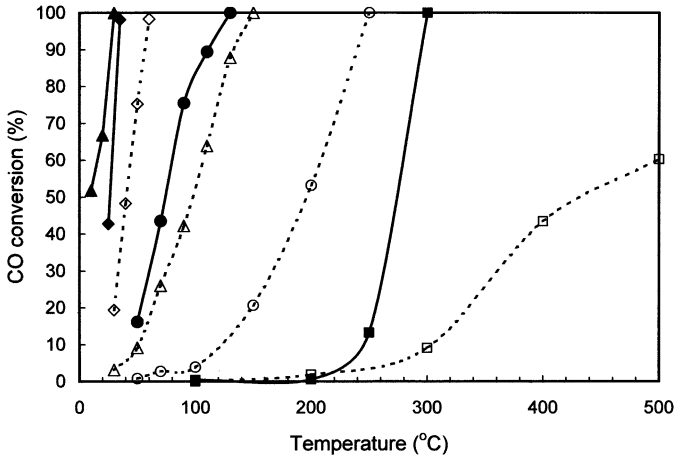

Fig. 5. CO oxidation activity of the catalysts. Full line, filled symbols—the HS series; dotted line, open symbols—the LS series. □, CeO_2-LS-300; ◇, Au/CeO_2-LS-300; △, Au/CeO_2-LS-500; ○, Au/CeO_2-LS-700; ■, CeO_2-HS-300; ◆, Au/CeO_2-HS-300; ▲, Au/CeO_2-HS-500; ●, Au/CeO_2-HS-700.

Au/CeO_2-HS-500 had only a band at 2154 cm^{-1} and a broad feature at 2130 cm^{-1}. The 2130 cm^{-1} band, also found with CeO_2-HS-300, was probably due to a physically adsorbed liquid like CO. The absence of the 2175 cm^{-1} band suggested that the Ce^{4+} sites were blocked when the gold-containing catalyst was calcined to 500 °C. Liu et al. predicted that gold atoms adsorb most strongly on Ce^{4+} ion at oxygen vacancy sites [38]. We suggest that the CO adsorbed at this type of site gave rise to the CO band at 2175 cm^{-1}. On calcination at 500 °C, gold atoms became mobile, and those migrating from particles on less energetically favored sites became trapped at these sites, hence inhibiting the adsorption of CO on these sites. The trapping of gold clusters at these sites might be responsible for the lower sintering suffered by gold supported on the high-surface area ceria.

Absorption bands due to chemisorbed CO on metallic gold could not be found on either gold catalyst. Weak adsorption of CO on oxidized gold/ceria catalysts was reported by Tabakova et al., who attributed this to the presence of adsorbed oxygen on small gold particles [39].

3.4. Catalytic activities

3.4.1. CO oxidation

The activity of the catalysts for CO oxidation as a function of the reaction temperature is shown in Fig. 5. The temperature at which the CO conversion reached 50% (T_{50}) is taken as a measure of the catalytic activity. Table 4 gives the T_{50} values, along with the rate of the reaction at 30 °C for some of the gold catalysts and at 300 °C for the gold-free ceria samples for comparison. Compared with titania-supported gold catalysts reported in the literature [40], the activity of the ceria-supported gold catalysts in this work is much lower for CO oxidation. Hence, whereas the T_{50} for the reference Au/TiO_2 catalyst should be at a subambient temperature of −45 °C, Au/CeO_2-HS-500, the most active catalyst in this investigation, required a temperature of 10 °C for 50% conversion. The data show that the CO oxi-

Table 4
Catalytic activity for CO oxidation

Catalyst	T_{50} (°C)	Rate of reaction at 30 °C ($mol\,s^{-1}\,g^{-1}$)	Rate of reaction at 300 °C ($mol\,s^{-1}\,g^{-1}$)
CeO_2-LS-300	430	–	1.6×10^{-7}
Au/CeO_2-LS-300	40	3.4×10^{-7}	–
Au/CeO_2-LS-500	97	5.4×10^{-8}	–
Au/CeO_2-LS-700	195	–	–
CeO_2-HS-300	274	–	1.7×10^{-6}
Au/CeO_2-HS-300	27	1.2×10^{-6}	–
Au/CeO_2-HS-500	10	1.7×10^{-6}	–
Au/CeO_2-HS-700	74	–	–
Au/TiO_2	−45[a]	–	–

Reaction conditions: 0.2 g catalyst, 1% CO in synthetic air at a total flow rate of 50 mL min^{-1}.
[a] Data from the catalyst supplier.

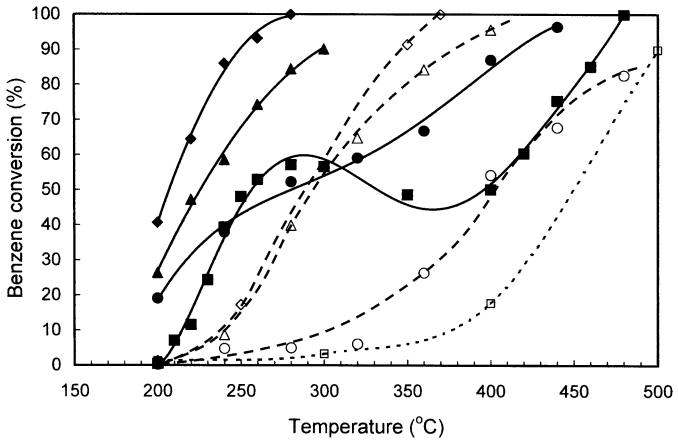

Fig. 6. Benzene oxidation activity of the catalysts. Full line, filled symbol—the HS series; dotted line, open symbol—the LS series. □, CeO_2-LS-300; ◇, Au/CeO_2-LS-300; △, Au/CeO_2-LS-500; ○, Au/CeO_2-LS-700; ■, CeO_2-HS-300; ◆, Au/CeO_2-HS-300; ▲, Au/CeO_2-HS-500; ●, Au/CeO_2-HS-700.

dation activity of ceria depends greatly on the catalyst surface area. At 300 °C, the rate of CO oxidation over CeO_2-HS-300 was 1.7×10^{-6} $mol\,s^{-1}\,g^{-1}$, about 10 times the value for CeO_2-LS-300. A large promotional effect of gold was found. The T_{50} value for Au/CeO_2-HS-300 was reduced to 27 °C from that of 274 °C for CeO_2-HS-300, and that for Au/CeO_2-LS-300 was reduced to 40 °C from that of 430 °C for CeO_2-LS-300. With the Au/CeO_2-LS catalyst series, the activity decreased with increasing calcination temperature. In contrast, maximum activity was found for the catalyst calcined at 500 °C for the Au/CeO_2-HS catalyst series.

3.4.2. Benzene oxidation

Carbon dioxide and water were the only products observed in the reaction. Carbon mass balance was very close to 100% under all conditions. The activity of the catalysts for benzene oxidation as a function of reaction temperature is shown in Fig. 6. Again, the activity of CeO_2-LS-300 was found to be much lower than that for CeO_2-HS-300. CeO_2-HS-300 showed a peculiar variation of activity with reaction temperature. At low temperature, benzene conversion increased with increasing reaction temperature up to 280 °C. Between 280 and 350 °C,

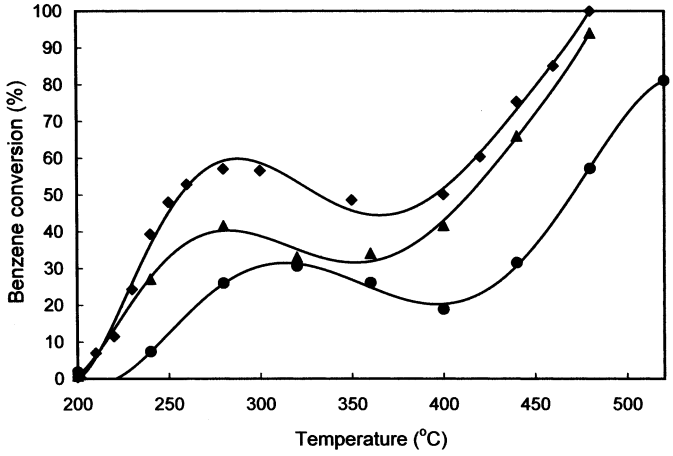

Fig. 7. Effect of calcination temperature on benzene oxidation activity of the precipitated ceria. ◆, CeO_2-HS-300; ▲, CeO_2-HS-500; ●, CeO_2-HS-700.

activity declined with increasing reaction temperature. Above 350 °C, the activity again increased with increasing temperature. The reaction was run with decreasing temperature immediately after the initial test with increasing temperature. The low-temperature conversion peak was again found, demonstrating that irreversible deactivation of the catalyst between 280 and 350 °C was not the cause of the peculiar behavior. The catalyst was also analyzed by in situ XRD while the catalyst was gradually heated from room temperature to 500 °C in a benzene–air mixture identical to that used for the oxidation reaction. No changes in the XRD pattern were detected, showing that reversible change in the bulk ceria sample did not occur under the reaction condition either.

Adding gold led to enhanced catalyst activity. Increasing calcination temperature led to decreased activity, so much so that the Au/CeO_2-HS-700 catalyst was less active than the pure support calcined at 300 °C (CeO_2-HS-300) in the temperature range 250–300 °C. The effect of sintering of the support alone is shown in Fig. 7. The activity of CeO_2-HS in both the low-temperature and high-temperature regimes was reduced by calcination at progressively higher temperature. The T_{50} values and rates of the benzene oxidation reaction at 250 °C are given in Table 5. The T_{50} value for CeO_2-HS-300 was that seen at low temperature. T_{50} values for CeO_2-HS-500 and CeO_2-HS-700 are not given, because the maximum conversion of these two samples did not exceed 50% in the low-temperature regime.

3.5. The effect the nature of the support on the structure and activity of gold

Although it is well documented that finely dispersed gold on reducible oxide support is important in producing highly active gold catalysts, the nature of the active gold species, whether ionic or metallic, has been disputed. On the basis of the decrease in activity concomitant with the reduction of oxidized gold, Park and Lee concluded that oxidized gold is more active on gold supported on Fe_2O_3, TiO_2, and Al_2O_3 [41]. Similarly, Guzman and Gate maintained that Au(I) is more active than

Table 5
Catalytic activity for benzene oxidation

Catalyst	T_{50} (°C)	Rate of reaction at 250 °C (mol s^{-1} g^{-1})
CeO_2-LS-300	450	7.9×10^{-8}
Au/CeO_2-LS-300	292	6.0×10^{-7}
Au/CeO_2-LS-500	299	5.6×10^{-7}
Au/CeO_2-LS-700	400	1.2×10^{-7}
CeO_2-HS-300	256	1.7×10^{-6}
CeO_2-HS-500	–	1.1×10^{-6}
CeO_2-HS-700	–	4.2×10^{-7}
Au/CeO_2-HS-300	207	3.1×10^{-6}
Au/CeO_2-HS-500	225	2.4×10^{-6}
Au/CeO_2-HS-700	280	1.5×10^{-6}
Au/TiO_2	363	–

Reaction conditions: 0.2 g catalyst, 0.5% benzene in synthetic air at a total flow rate of 200 mL min^{-1}.

Au(0) for CO oxidation [42,43]. Based on XPS results and the retention of catalytic activity after metallic gold was stripped from the Au/CeO_2 catalysts, Fu et al. maintained that Au^+ was the active species for the water–gas shift gas reaction [44]. On the basis of the much higher activity for ceria-supported gold prepared by deposition–precipitation compared with that prepared by solvated metal atom dispersion, Venezia et al. argued that ionic gold substituted into the lattice of ceria should be much more active than metallic gold [32]. But Haruta et al. disputed the role of oxidic gold [45], on the grounds that most XPS results showed the presence of metallic gold in the most active gold catalysts [46,47]. These authors also asserted that oxidic gold should be reduced under the CO oxidation conditions. Instead of considering either metallic or ionic gold as the only active species, Bond and Thompson proposed a scheme in which both Au^0, which adsorbs CO, and Au(III), which cements the metallic particles on the support and activates surface hydroxy groups for reaction with the adsorbed CO to form adsorbed carboxylate, are required for high activity. According to this mechanism, carbon dioxide is formed from the reaction of the carboxylate by superoxide ions adsorbed on oxygen vacancy sites on the support oxide [48]. Kung et al. proposed that an ensemble of Au(I)–OH and metallic gold is the active species for CO oxidation of Au/γ-Al_2O_3 [49,50]. In the present study we have observed that the structure of the gold particle depends strongly on the nature of the ceria support. By XPS, we observed that oxidic gold comprised about 10% of the total gold in the Au/CeO_2-HS samples but only a negligible percentage in the Au/CeO_2-LS samples. The fraction of oxidic to metallic gold hardly changed when the Au/CeO_2-HS-300 was used for the CO oxidation reaction. The high-surface area ceria was able to stabilize small gold particles and also maintain a fraction of the deposited gold in the oxidic state. Based on the FTIR results for adsorbed CO, it is reasonable to assume that low-coordination ceria sites in association with an oxygen vacancy sites are responsible for the strong binding of small gold particles. The weaker surface Ce–O bonding revealed by TPR can account for the easier generation of these sites on the high-surface area ceria. However, the activity data do not allow us to draw any conclusions about the nature of the active gold species. Both gold catalyst series are quite active for CO oxidation. Because cationic gold was found on the HS catalyst series but not on the LS catalyst series, it may be argued that the comparatively higher activity of the HS catalyst series was due to the higher activity of the cationic gold. But the gold particle size on the Au/CeO_2-LS series is larger, as evidenced by TEM. Hence the lower activity of the AuCeO_2-LS catalysts may also be interpreted as resulting from particle size effect. For CO oxidation, the optimum activity found for the HS series gold catalyst calcined at 500 °C probably reflects the fact that CO activation depends critically on the structure of the gold nanoparticles. The gold particle size in Au/CeO_2-HS-300 was probably too small. An optimum structure was reached after calcination of the catalyst at 500 °C. With the LS catalyst series, the gold particle sizes were larger, greatly exceeding the optimum size, and so calcination of the catalysts at increasing temperature could only lead to decreased activity.

For benzene oxidation, the effect of the support is more profound. The low-temperature benzene oxidation activity found for CeO_2-HS-300 below 300 °C was absent for CeO_2-LS-300. Zhao and Gorte reported on the presence of both a low-temperature process and a high-temperature process for the oxidation of propane and *n*-butane on ceria prepared by decomposition of $Ce(NO_3)_3 \cdot H_2O$, which gave CeO_2 with a specific surface area of 61 m^2 g^{-1} [51]. Based on the dependence of the rate of the reaction to oxygen partial pressure, these authors proposed that dissociatively adsorbed oxygen is involved in the low-temperature reaction of *n*-butane. The low-temperature benzene oxidation reaction observed here could be interpreted as the reaction of adsorbed benzene with an adsorbed oxygen species. Between 200 and 300 °C, thermal activation of the adsorbed species was rate-limiting, and the reaction rate increased with increasing temperature. Between 300 and 400 °C, desorption of the adsorbed species caused the decrease in reactivity with temperature. Above 400 °C, benzene oxidation proceeded with the lattice oxygen in accordance with the Mars van Krevelan mechanism. The difference in the behavior of the CeO_2-LS and CeO_2-HS samples suggested that the surface reaction is effective only over ceria of small particle size. This difference is related to the higher reducibility of the surface oxygen. It has often been postulated that oxygen vacancy sites, generated along with the reduction of Ce^{4+} to Ce^{3+}, are sites for oxygen adsorption, forming reactive oxygen species. Li et al. proposed that surface peroxo were responsible for the oxidation of hydrocarbons on ceria below 300 °C [16]. Pushkarev et al. detected superoxo and peroxo species only on nanocrystalline ceria prereduced by exposure to hydrogen or carbon monoxide [52]. Guzman et al. found that on gold/ceria samples, superoxo and peroxo species were detected when nanocrystalline ceria was used as a support, but not when large-sized ceria was used [53]. We postulate that oxygen vacancy sites were generated as the catalyst is heated in the benzene air mixture. Once generated, these acted as sites for the adsorption of superoxo and peroxo species, which were thermally decomposed to form reactive oxygen responsible for the low-temperature oxidation of benzene. On the low-surface area ceria, these processes occur at much higher temperatures, at which the lattice oxygen became

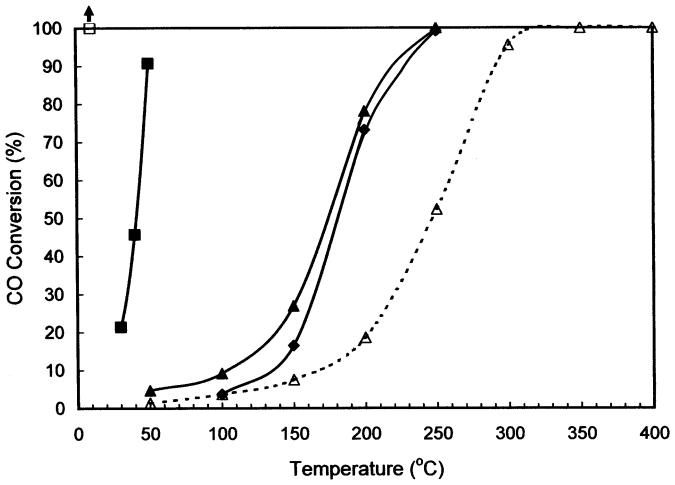

Fig. 8. Conversion of CO over the reactivated Au/CeO_2-HS-500 catalyst (full line, filled symbol) and the reference Au/TiO_2 catalysts (dotted line, open symbol) with different reactant composition. ■,□, 1% CO in air, total gas flow rate at 50 mL min^{-1}; ◆, 1% CO and 0.5% C_6H_6 in air, total gas flow rate at 200 mL min^{-1}; ▲,△, 1% CO, 0.5% C_6H_6 and 3% H_2O in air, total flow rate at 200 mL min^{-1}.

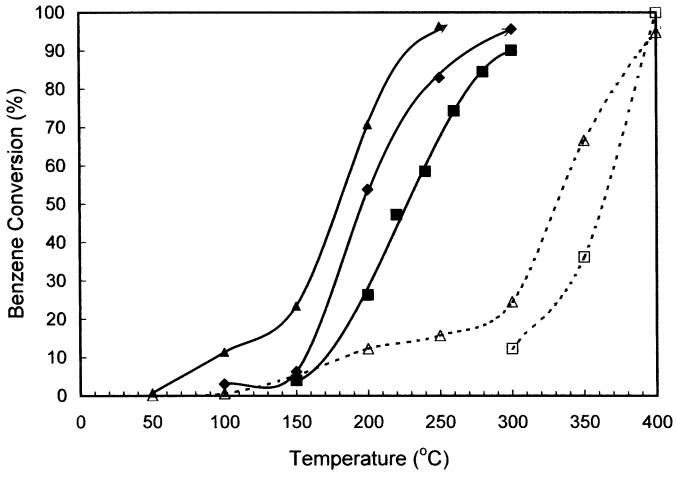

Fig. 9. Conversion of C_6H_6 over the reactivated Au/CeO_2-HS-500 catalyst (full line, filled symbol) and the reference Au/TiO_2 catalysts (dotted line, open symbol) with different reactant composition. ■,□, 0.5% C_6H_6 in air, total gas flow rate at 200 mL min^{-1}; ◆, 1% CO and 0.5% C_6H_6 in air, total gas flow rate at 200 mL min^{-1}; ▲,△: 1% CO, 0.5% C_6H_6 and 3% H_2O in air, total flow rate at 200 mL min^{-1}.

appreciably mobile. For benzene oxidation, the activation of benzene probably occurs on the ceria surface. The function of gold is secondary, aiding the dissociation of the surface oxygen species. The presence of high-surface area nanocrystalline ceria is most important for low-temperature benzene oxidation activity. This then accounts for the observation that below 300 °C, all of the LS series catalysts, even after the addition of gold, were less active than the gold-free high-surface area sample CeO_2-300. Even with the HS catalyst series, Au/CeO_2-HS-700 was less reactive than CeO_2-HS-300 in the temperature range 250–300 °C. Sintering of the ceria, evident by the lower surface area of the catalyst calcined at 700 °C, had a significant effect on activity. In contrast, even the least active gold-containing catalyst was more active than both ceria samples for CO oxidation. The activation of carbon monoxide on nanogold particles is essential for low-temperature CO oxidation.

3.6. Catalyst stability

All of the catalysts showed negligible change in activity over a time on stream of 6 h. But when the catalysts were stored under ambient conditions for 3 months, the activity for CO oxidation decreased. The T_{50} for Au/CeO_2-HS-500 increased from 10 to 56 °C. The activity was restored to a certain extent by calcination in air at 500 °C for 2 h. The T_{50} for the reactivated catalyst was 41 °C, still lower than that of the fresh catalyst.

3.7. Activity of the catalysts in a mixture of CO, benzene and moisture

The activities of the reactivated Au/CeO_2-HS-500 and the reference Au/TiO_2 catalyst, in a reaction mixture of 0.5% benzene and 1% CO, with or without 3% water vapor, are shown in Figs. 8 and 9. For comparison, the activities of the catalysts for CO oxidation and benzene oxidation when the reactant was present alone in air are also shown in the corresponding figures. CO oxidation on Au/CeO_2 was significantly inhibited by benzene. The T_{50} for CO increased from 41 to 180 °C in the presence of benzene. Adding water vapor had a small beneficial effect on the oxidation of CO in the gas mixture, lowering T_{50} slightly, to 175 °C. In contrast, although the Au/TiO_2 reference catalyst is very active for CO oxidation, it is much less active for benzene oxidation, and its CO oxidation activity is greatly suppressed by benzene. At 10 °C, the lowest temperature used in this work, CO was completely converted over Au/TiO_2. (The T_{50} for CO oxidation given by the catalyst suppler was −45 °C.) In the CO–benzene–water–air mixture, the T_{50} for CO oxidation increased to 245 °C. On both catalysts, the adsorption of benzene to high coverage at low temperature inhibited the adsorption and reaction of CO. CO oxidation was effective only at temperatures at which desorption or reaction of benzene became significant, freeing some sites for the reaction of CO. The lower activity of Au/TiO_2 for benzene oxidation means that higher temperatures are required to remove benzene, and so this catalyst is less active than Au/CeO_2-HS-500 in the gas mixture for both CO and benzene oxidation.

Fig. 9 shows that whereas CO oxidation was inhibited by benzene, benzene oxidation was enhanced by CO. If CO and benzene were competing for the same sites, then one would expect the activity of benzene to be hardly affected, because of its much stronger adsorption. The enhanced benzene oxidation suggested that additional oxygen species reactive toward benzene oxidation were produced by CO oxidation.

The mechanism of CO oxidation has been extensively debated. Over transition metal oxides such as Fe_2O_3 and TiO_2, Haruta et al. proposed that peroxo species adsorbs on metal oxide sites and then reacts with CO adsorbed on the gold sites at the metal–oxide perimeter [54]. Based on isotope scrambling experiments on Au/Fe_2O_3, Schubert et al. suggested that oxygen adsorbs molecularly on the support but dissociates on gold before reaction with CO [55]. Using theoretical simula-

tion, Sanchez et al. noted that O_2 adsorbs as an activated peroxo species that can react with both gaseous-phase and adsorbed CO on gold clusters deposited on MgO [56,57]. The formation of peroxo species on Au_n^- ($n < 20$) clusters, where n is even, was also detected experimentally [58]. The adsorption of CO and O_2 on gaseous Au_n^- clusters was found to be cooperative rather than competitive [59]. Stolcic et al. proposed that on small gold catalysts, the adsorbed peroxo species further react with CO, yielding the gaseous product CO_2 and an adsorbed oxygen atom [58]. The results found in this study support the mechanism that CO oxidation occurs by the reaction between CO and a nondissociated adsorbed oxygen at the gold–support boundary, producing CO_2 and a highly reactive atomic oxygen species. The activated atomic oxygen can then react with both CO and benzene.

An enhanced rate of CO oxidation on gold catalysts due to moisture has been observed [41,60–63]. It has been suggested that water vapor aids the dissociation of molecular oxygen [41, 61,62,64] as well as the decomposition of carbonate [61,63]. A clearer picture of the effect of water was revealed by first-principle calculation, demonstrating that coadsorption of water with oxygen on either small free gold clusters or small gold clusters supported on defect-free MgO(100) resulted in partial or complete transfer of the proton to the oxygen, giving rise to a hydroperoxyl-like complex with a weak O–O bond [65]. Thus, normally nonreactive gold clusters are activated by adsorbed water. Our observation that water vapor promoted both CO and benzene oxidation on reactivated Au/CeO_2-HS-500 gives further support to the mechanism that considers the effect of water to be oxygen activation, which is required for both CO and benzene oxidation on nanogold particles.

4. Conclusion

High-surface area ceria prepared by precipitation and calcination at only low temperatures showed high surface reducibility and high activity for benzene oxidation at low temperatures. The high-surface area ceria can stabilize gold at high dispersion. Highly dispersed gold promotes the oxidation of CO and benzene, by activating CO in the former case and by assisting the dissociation of adsorbed oxygen in the latter. The performance of gold supported on high-surface area ceria for the oxidation of a mixture of CO and benzene is superior to that of gold supported on titania, despite the excellent activity of titania-supported gold catalyst for low-temperature CO oxidation. At 250 °C, both CO and benzene conversion were >90%. Because moisture is beneficial to oxidation activity, ceria-supported gold is a promising catalyst for pollution abatement in ambient air.

References

[1] M. Haruta, N. Yamada, T. Kobayashi, S. Ijima, J. Catal. 115 (1989) 301.
[2] M. Haruta, Catal. Today 36 (1997) 153.
[3] G.C. Bond, D.T. Thompson, Catal. Rev.-Sci. Eng. 41 (1999) 319.
[4] G.J. Hutchings, Gold Bull. 37 (2004) 3.
[5] C. Milone, R. Ingoglia, A. Pistone, C. Crisafulli, G. Neri, S. Galvagno, Book of Abstracts, Vol. 2, 2004, p. 265.
[6] P. Claus, Appl. Catal. A 291 (2005) 222.
[7] G.K. Bethke, H.H. Kung, Appl. Catal. A 194–195 (2000) 43.
[8] M.M. Schubert, V. Plzak, J. Garche, R.J. Behm, Catal. Lett. 76 (2001) 143.
[9] P. Landon, P.J. Collier, A.J. Papworth, C.J. Kiely, G.J. Hutchings, Chem. Commun. (2002) 2058.
[10] T. Hayashi, K. Tanaka, M. Haruta, J. Catal. 178 (1998) 566.
[11] Y.-H. Yuan, X.-G. Zhou, W. Wu, Y.-R. Zhang, W.-K. Yuan, L. Luo, Catal. Today 105 (2005) 544.
[12] Q. Fu, A. Weber, M. Flytzani-Stephanopoulos, Catal. Lett. 77 (2001) 87.
[13] D. Andreeva, V. Idakiev, T. Tabakova, L. Ilieva, P. Falaras, A. Bourlinos, A. Travlos, Catal. Today 72 (2002) 51.
[14] J.R. Mellor, A.N. Palazov, B.S. Grigorova, J.F. Greyling, K. Reddy, M.P. Letsoalo, J.H. Marsh, Catal. Today 72 (2002) 145.
[15] A.C. Gluhoi, S.D. Lin, B.E. Nieuwenhuys, Catal. Today 90 (2004) 175.
[16] C. Li, Q. Xin, X. Guo, T. Onishi, New Frontiers in Catalysis, Part C, Elsevier, 1993, pp. 1955–1958.
[17] M.A. Hasan, M.I. Zaki, L. Pasupulety, J. Phys. Chem. B 106 (2002) 12747.
[18] Y.-W. Zhang, R. Si, C.-S. Liao, C.-H. Yan, C.-X. Xiao, Y. Kou, J. Phys. Chem. B 107 (2003) 10159.
[19] M.A. Centeno, M. Paulis, M. Montes, J.A. Odriozola, Appl. Catal. A 234 (2002) 65.
[20] S. Scirè, S. Minicò, C. Crisafulli, C. Satriano, A. Pistone, Appl. Catal. B 40 (2003) 43.
[21] S. Minicò, S. Scirè, C. Crisafulli, R. Maggiore, S. Galvagno, Appl. Catal. B 28 (2000) 245.
[22] V. Idakiev, L. Ilieva, D. Andreeva, J.L. Blin, L. Gigot, B.L. Su, Appl. Catal. A 243 (2003) 25.
[23] D. Andreeva, R. Nedyalkova, L. Ilieva, M.V. Abrashev, Appl. Catal. A 246 (2003) 29.
[24] H. Cordatos, T. Bunluesin, J. Stubenrauch, J.M. Vohs, R.J. Gorte, J. Phys. Chem. 100 (1996) 785.
[25] S. Carrettin, P. Concepción, A. Corma, J.M.L. Nieto, V.F. Puntes, Angew. Chem. Int. Ed. 43 (2004) 2538.
[26] J. Fisher, Gold Bull. 36 (2003) 155.
[27] G.M. Ingo, E. Paparazzo, O. Bagnarelli, N. Zacchetti, Surf. Interface Anal. 16 (1990) 515.
[28] A.M. Salvi, F. Decker, F. Varsano, G. Speranza, Surf. Interface Anal. 31 (2001) 255.
[29] D. Briggs, M.P. Seah, Practical Surface Analysis, X-Ray Photoelectron Spectroscopy, Vol. 1, Wiley, 1990, pp. 593–625.
[30] S. Arrii, F. Morfin, A.J. Renouprez, J.L. Rousset, J. Am. Chem. Soc. 126 (2004) 1199.
[31] H.C. Yao, Y.F.Y. Yao, J. Catal. 86 (1984) 254.
[32] A.M. Venezia, G. Pantaleo, A. Longo, G.D. Carlo, M.P. Casaletto, F.L. Liotta, G. Deganello, J. Phys. Chem. B 109 (2005) 2821.
[33] H. Cordatos, D. Ford, R.J. Gorte, J. Phys. Chem. 100 (1996) 18128.
[34] T.X.T. Sayle, S.C. Parker, D.C. Sayle, Phys. Chem. Chem. Phys. 7 (2005) 2936.
[35] A.C. Gluhoi, H.S. Vreeburg, J.W. Bakker, B.E. Nieuwenhuys, Appl. Catal. A 291 (2005) 145.
[36] C. Binet, M. Daturi, J.-C. Lavalley, Catal. Today 50 (1999) 207.
[37] A. Badri, C. Binet, J.-C. Lavalley, J. Phys. Chem. 100 (1996) 8363.
[38] A.-P. Liu, S. Jenkins, J.D.A. King, Phys. Rev. Lett. 94 (2005) 196102.
[39] T. Tabakova, F. Boccuzzi, M. Manzoli, D. Andreeva, Appl. Catal. A 252 (2003) 385.
[40] F. Moreau, G.C. Bond, A.O. Taylor, J. Catal. 231 (2005) 105.
[41] E.D. Park, J.S. Lee, J. Catal. 186 (1999) 1.
[42] J. Guzman, B.C. Gates, J. Am. Chem. Soc. 126 (2004) 2672.
[43] J. Guzman, B.C. Gates, J. Phys. Chem. B (2002) 7659.
[44] Q. Fu, H. Saltsburg, M. Flytzani-Stephanopoulos, Science (2003).
[45] M. Haruta, Chem. Record 3 (2003) 75.
[46] J.-D. Grunwaldt, M. Maciejewski, O.S. Becker, P. Fabrizioli, A. Baiker, J. Catal. 186 (1999) 458.
[47] L. Guczi, D. Horváth, Z. Pászti, L. Tóth, Z.E. Horváth, A. Karacs, G. Petõ, J. Phys. Chem. B 104 (2000) 3183.
[48] G.C. Bond, D.T. Thompson, Gold Bull. 33 (2000) 41.
[49] C.K. Costello, M.C. Kung, H.S. Oh, Y.M. Wang, H.H. Kung, Appl. Catal. A 232 (2002) 159.
[50] L. Fu, N.Q. Wu, J.H. Yang, F. Qu, D.L. Johnson, M.C. Kung, H.H. Kung, V.P. Dravid, J. Phys. Chem. B 109 (2005) 3704.

[51] S. Zhao, R.J. Gorte, Appl. Catal. A 277 (2003) 129.
[52] V.V. Pushkarev, V.I. Kovalchuk, J.L. D'Itri, J. Phys. Chem. B 108 (2004) 5341.
[53] J. Guzman, S. Carrettin, A. Corma, J. Am. Chem. Soc. 127 (2005) 3286.
[54] M. Haruta, S. Tsubota, T. Kobayashi, H. Kageyama, M.J. Genet, B. Delmon, J. Catal. 144 (1993) 175.
[55] M.M. Schubert, S. Hackenberg, A.C. van Veen, M. Muhler, V. Plzak, R.J. Behm, J. Catal. 197 (2001) 113.
[56] A. Sanchez, S. Abbet, U. Heiz, W.-D. Schneider, H. Hakkinen, R.N. Barnett, U. Landman, J. Phys. Chem. A 103 (1999) 9573.
[57] H. Hakkinen, S. Abbet, A. Sanchez, U. Heiz, U. Landman, Angew. Chem. Int. Ed. 42 (11) (2003) 1297–1300; 42 (2003) 1297.
[58] D. Stolcic, M. Fischer, G. Gantefor, Y.D. Kim, Q. Sun, P. Jena, J. Am. Chem. Soc. 125 (2003) 2848.
[59] W.T. Wallace, R.L. Whetten, J. Am. Chem. Soc. 124 (2002) 7499.
[60] F. Boccuzzi, A. Chiorino, J. Phys. Chem. B 104 (2000) 5414.
[61] M. Date, M. Okumura, S. Tsubota, M. Haruta, Angew. Chem. Int. Ed. 43 (2004) 2129.
[62] F. Boccuzzi, A. Chiorino, M. Manzoli, P. Lu, T. Akita, S. Ichikawa, M. Haruta, J. Catal. 202 (2001) 256.
[63] M.M. Schubert, A. Venugopal, M.J. Kahlich, V. Plzak, R.J. Behm, J. Catal. 222 (2004) 32.
[64] M. Daté, M. Haruta, J. Catal. 201 (2001) 221.
[65] A. Bongiorno, U. Landman, Phys. Rev. Lett. 95 (2005) 106102.